tektonika

Supporting Information
For
Bayesian estimation of surface strain rates in the peri-Adriatic, Balkans and Aegean region from GNSS velocities

M. Métois[1]*, C. Lasserre[1], A.Meridi[1], M.Henriquet[2], & T.Bodin[3]

[1]*Université Claude Bernard Lyon 1, ENS de Lyon, Université Jean Monnet, CNRS, LGL-TPE, UMR5276*
[2]*Université Côte d'Azur, IRD, CNRS, Observatoire de la Côte d'Azur, Geoazur, Valbonne, France.*
[3]*Institute of Marine Sciences (ICM-CSIC), Barcelona, Spain*
**Corresponding author (e-mail: marianne.metois@univ-lyon1.fr)*

This document presents supplementary figures associated with the paper "Bayesian estimation of surface strain rates in the peri-Adriatic, Balkans and Aegean region from GNSS velocities". We recall that the original velocity field comes from supplementary materials from (Piña-Valdés et al., 2022). The B-Strain outputs associated with this work are available on the EaSyData repository (DOI https://doi.org/10.57932/75c45007-1832-4d07-ad9f-cefe5dc1119d), and could be explored online on the BStrain Plotter webtool https://bstrainplotter.univ-lyon1.fr/home.

References

Gordon, R. G. and Houseman, G. A. (2015). Deformation of indian ocean lithosphere: Evidence for a highly nonlinear rheological law. Journal of Geophysical Research: Solid Earth, 120(6):4434–4449.

Piña-Valdés, J., Socquet, A., Beauval, C., Doin, M.-P., D'Agostino, N., and Shen, Z.-K. (2022). 3d gnss velocity field sheds light on the deformation mechanisms in europe: Effects of the vertical crustal motion on the distribution of seismicity. Journal of Geophysical Research: Solid Earth, 127(6):e2021JB023451.

Serpelloni, E., Cavaliere, A., Martelli, L., Pintori, F., Anderlini, L., Borghi, A., Randazzo, D., Bruni, S., Devoti, R., Perfetti, P., et al. (2022). Surface velocities and strain-rates in the euro-mediterranean region from massive gps data processing. Frontiers in Earth Science, 10:907897.

Tape, C., Musé, P., Simons, M., Dong, D., and Webb, F. (2009). Multiscale estimation of gps velocity fields. Geophysical Journal International, 179(2):945–971.

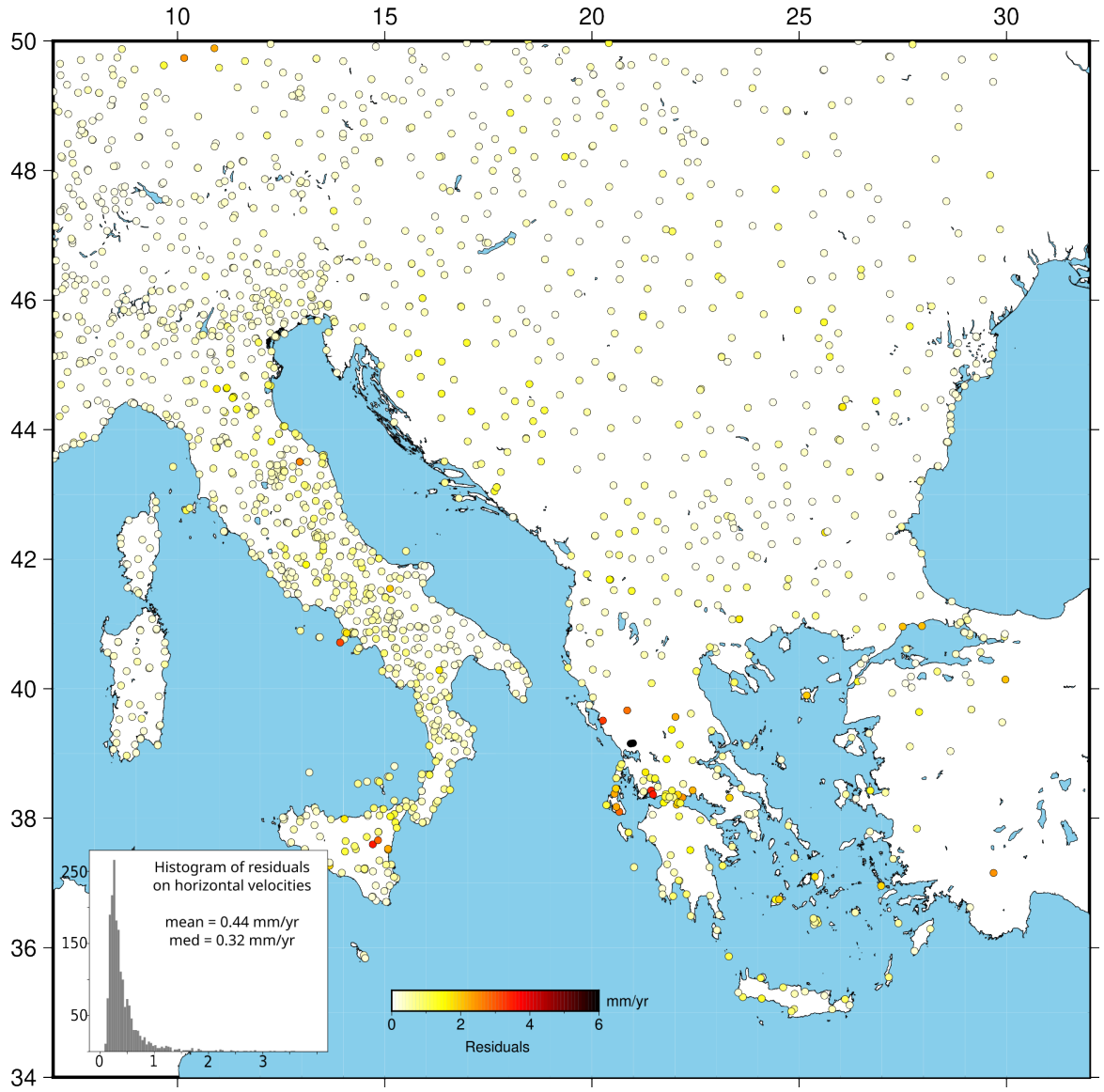

Fig. S1: Residuals between the observed horizontal velocities and predicted ones based on the interpolated velocity field (median of the PDF). Histogram of these residuals is presented in the inset

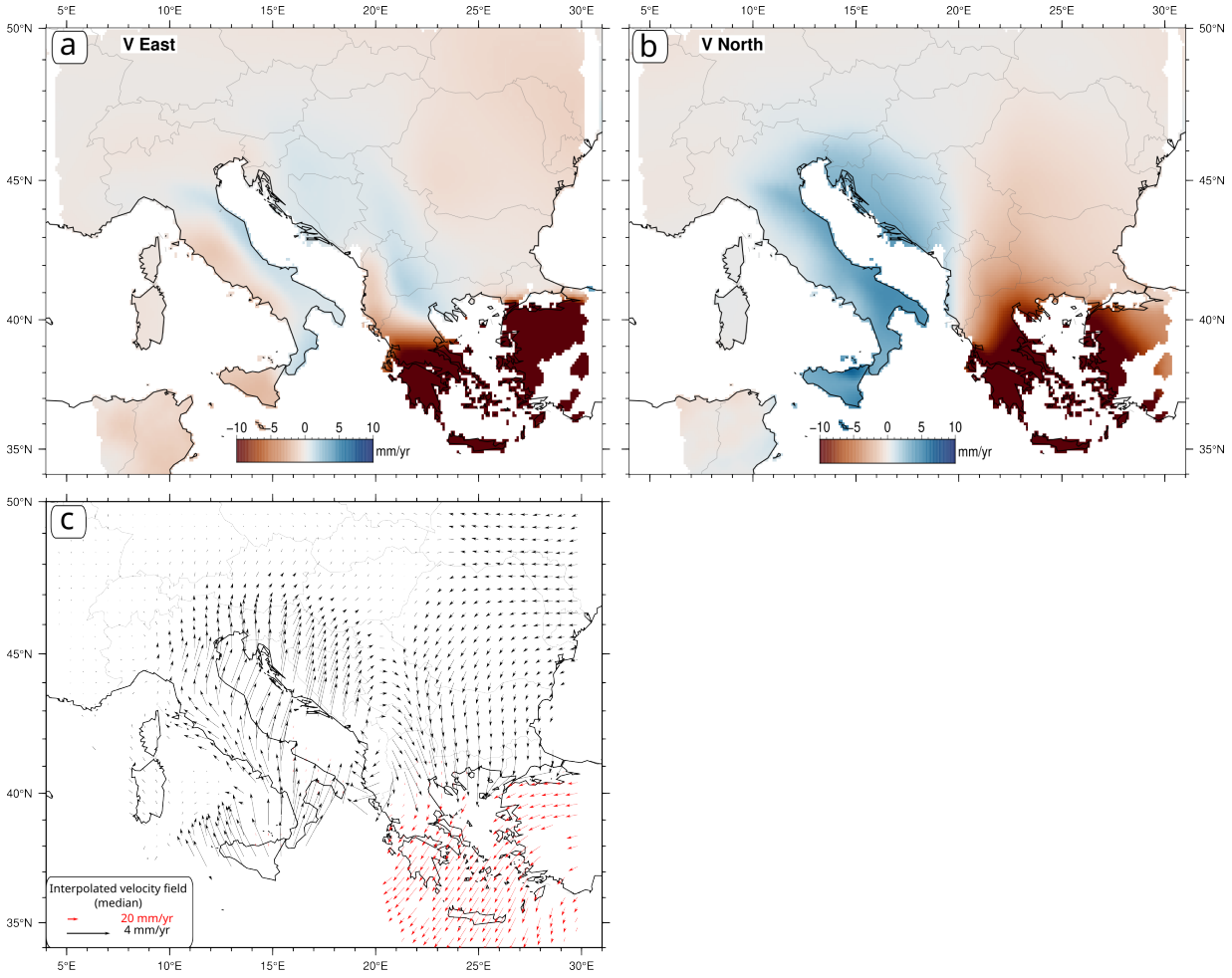

Fig. S2: a-b Median value of the interpolated horizontal components (East and North, respectively) of the velocity field in the Eurasia fixed reference frame, c-decimated interpolated velocity field.

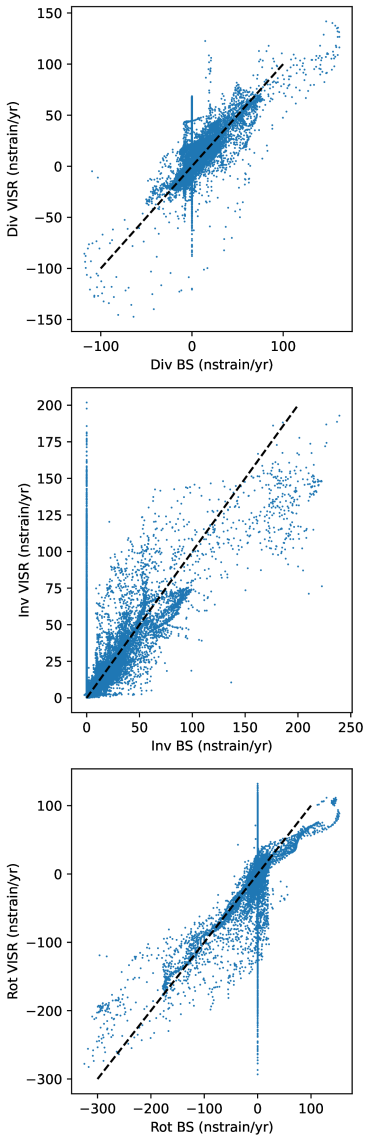

Fig. S3: Scatter plots presenting a pixel to pixel comparison of PDF's median values from our study to results from (Piña-Valdés et al., 2022) and the VISR3D method. The dashed black line is a 1:1 regression line. Pixels that fall in our low-resolution area, as defined by the standard deviation of the horizontal velocity higher than 3 mm/yr (green contours in figure 4 in the main text), have been disregarded.

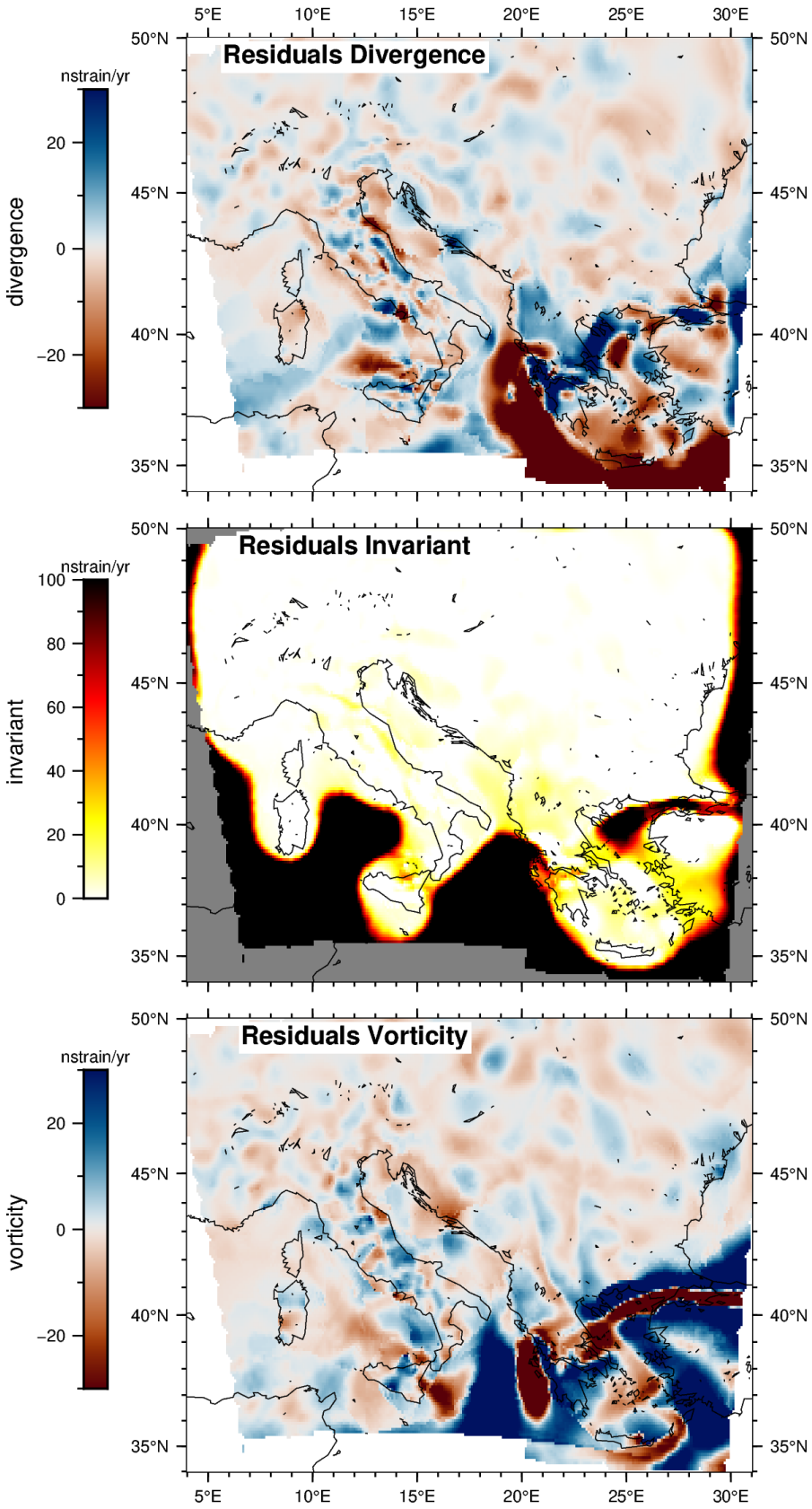

Fig. S4: Map views of the residuals observed between the divergence, second invariant, and vorticity calculated by the B-Strain and the VISR3D method. Color scales are the same as in figure 3 and 4 for comparison (see main text).

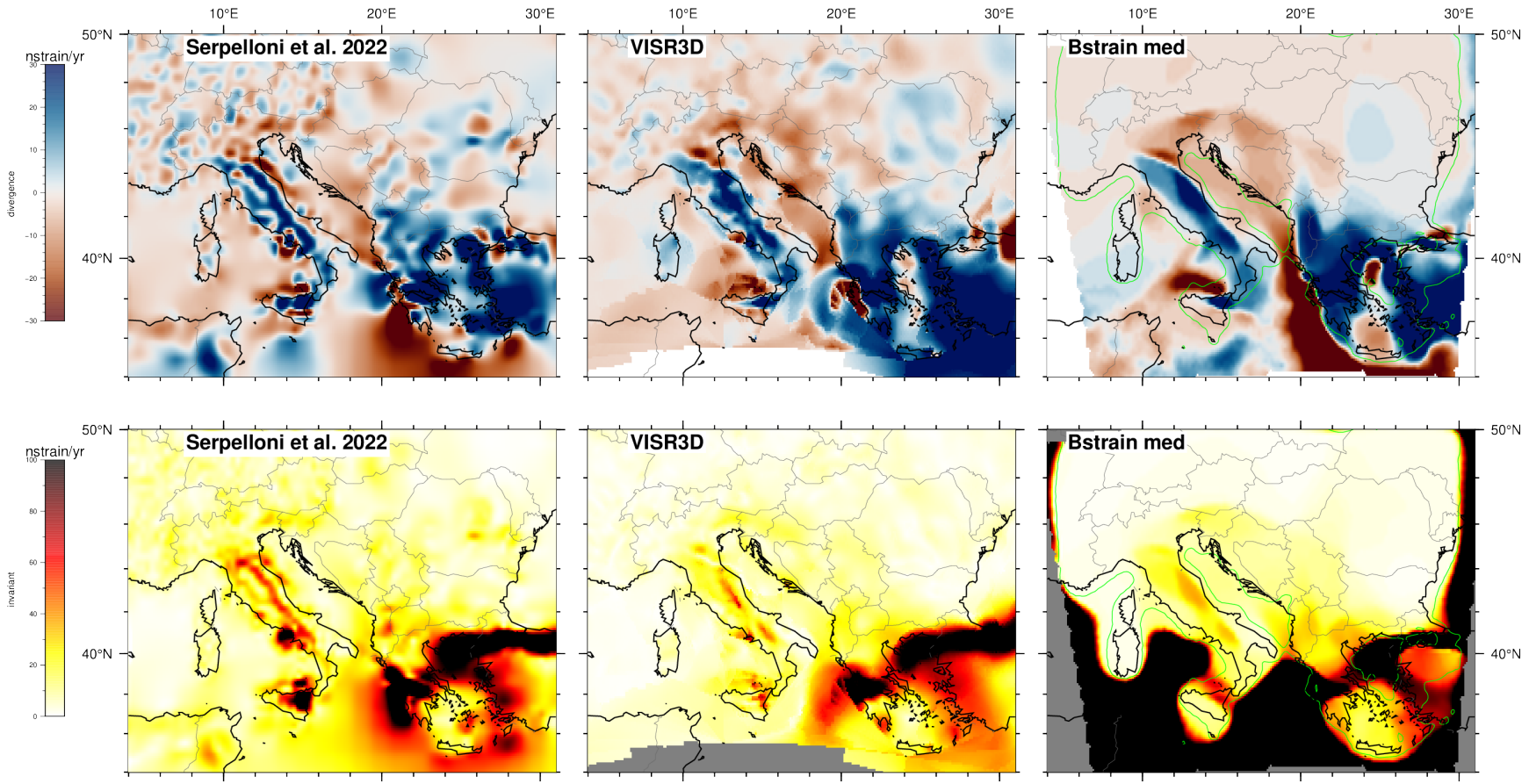

Fig. S5: Maps of the divergence (top) and second invariant (bottom) of the velocity field in the study area, obtained using the wavelet-based method from (Tape et al., 2009) (left, (Serpelloni et al., 2022)), the VISR3D interpolation method (center, Piña-Valdés et al. (2022)) and the B-Strain inversion method (right, median of the PDF from *this study*).

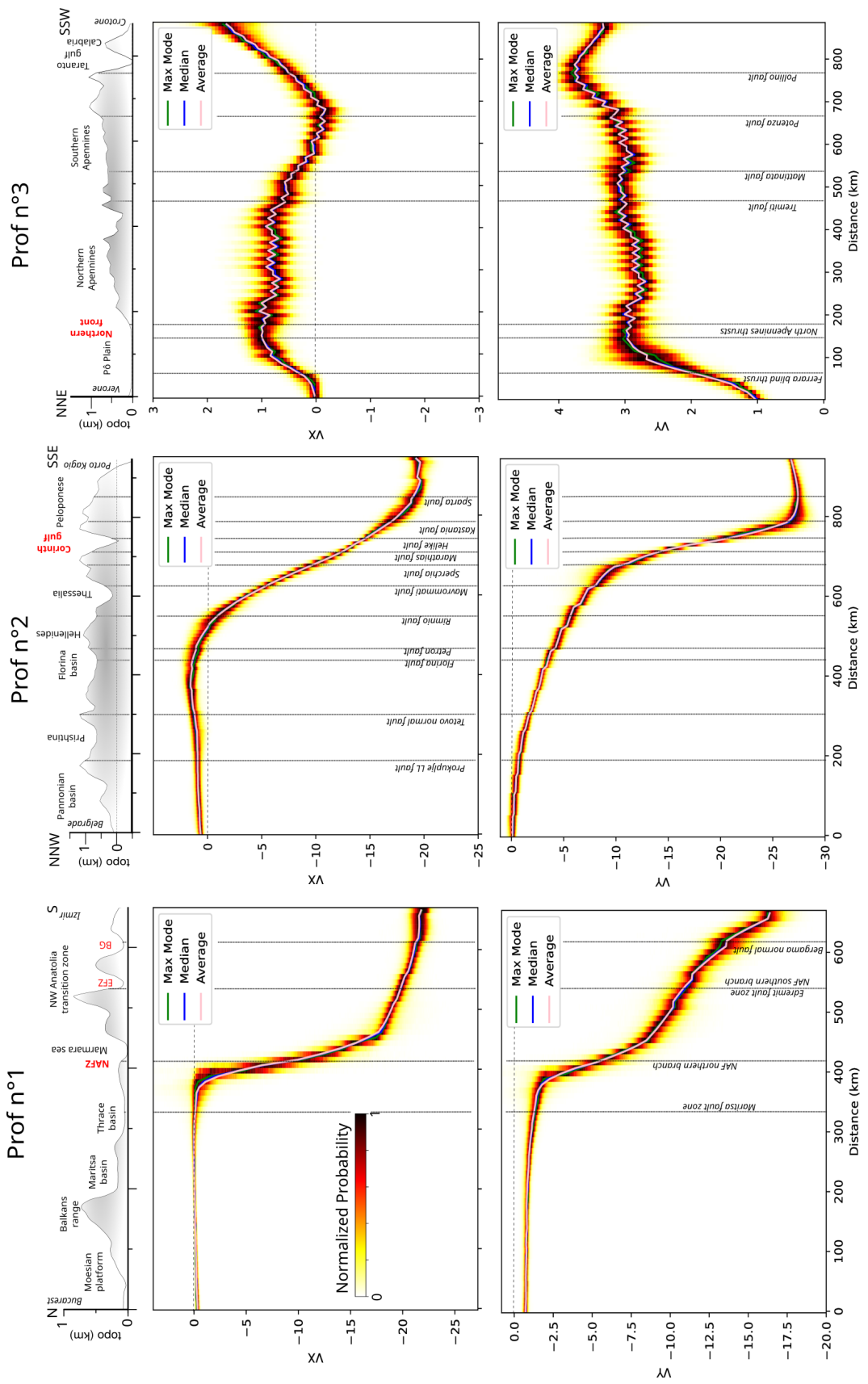

Fig. S6: Same than figure 5 but for East and North component of the velocity and with PDF normalized based on their maximum value.

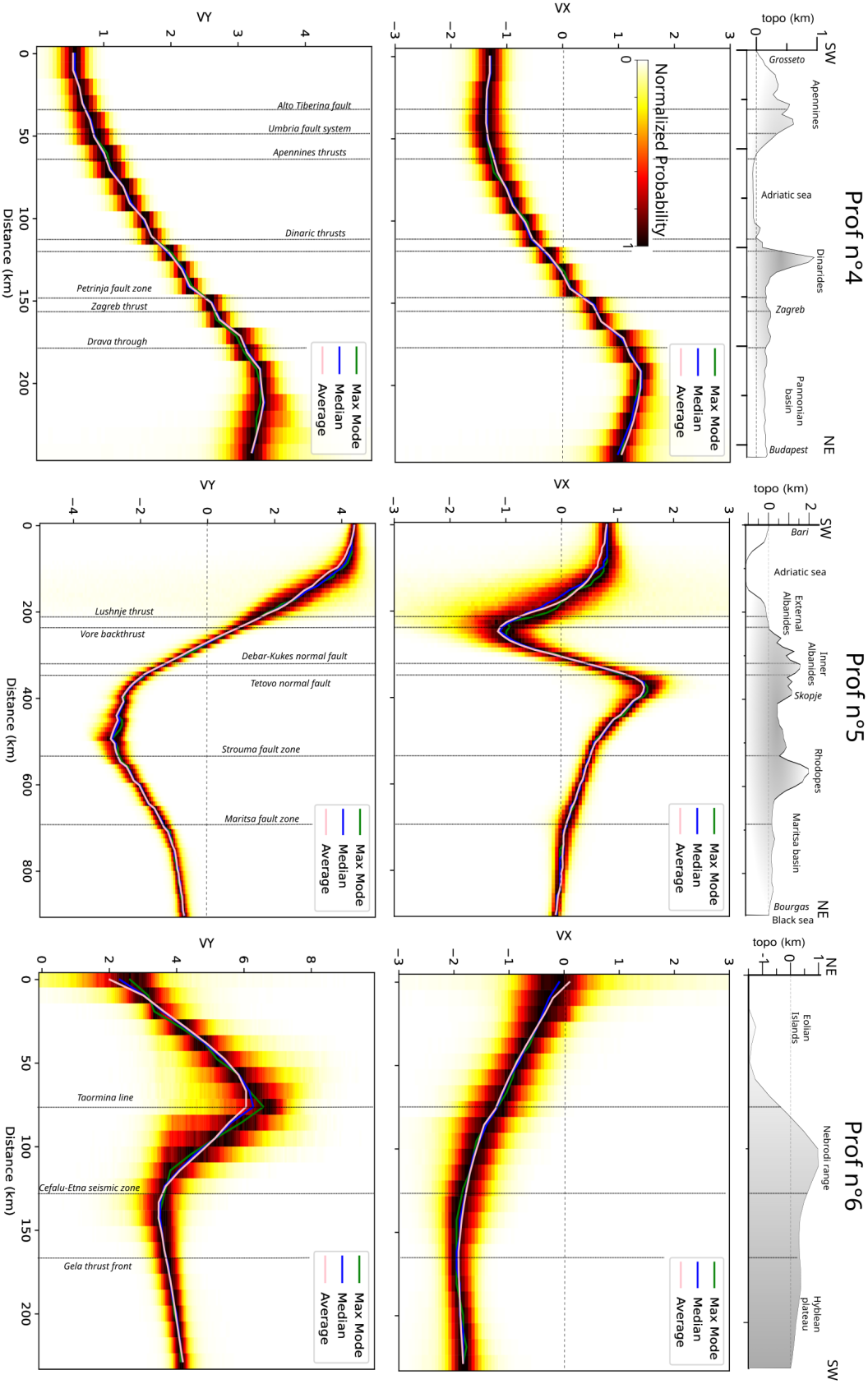

Fig. S7: Same than figure 6 but for East and North component of the velocity and with PDF normalized based on their maximum value.

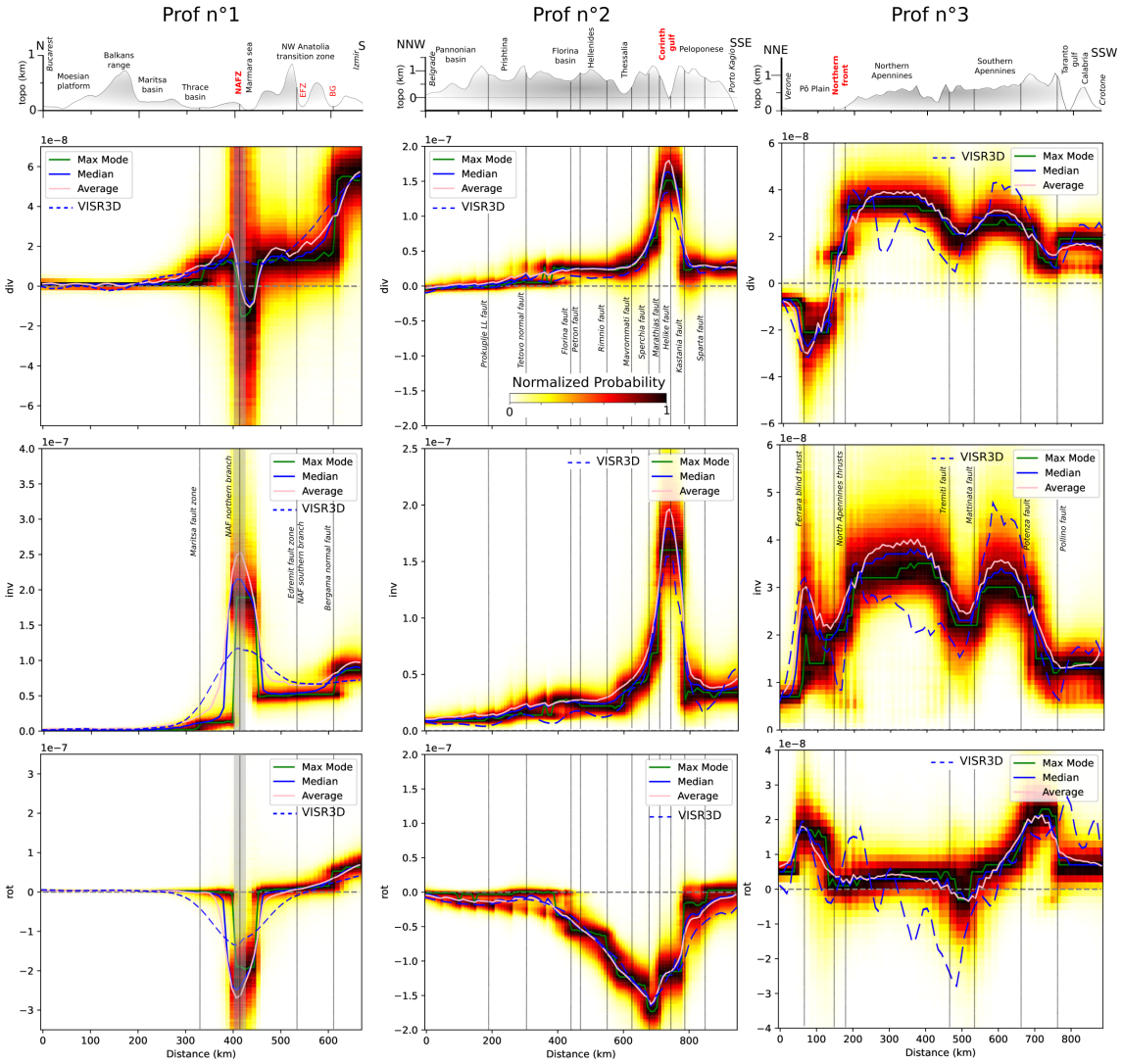

Fig. S8: Same than figure 5 but with PDF normalized based on their maximum value rather than on its integral. I.e. whatever the considered pixel, the PDF ranges between 0 and 1.

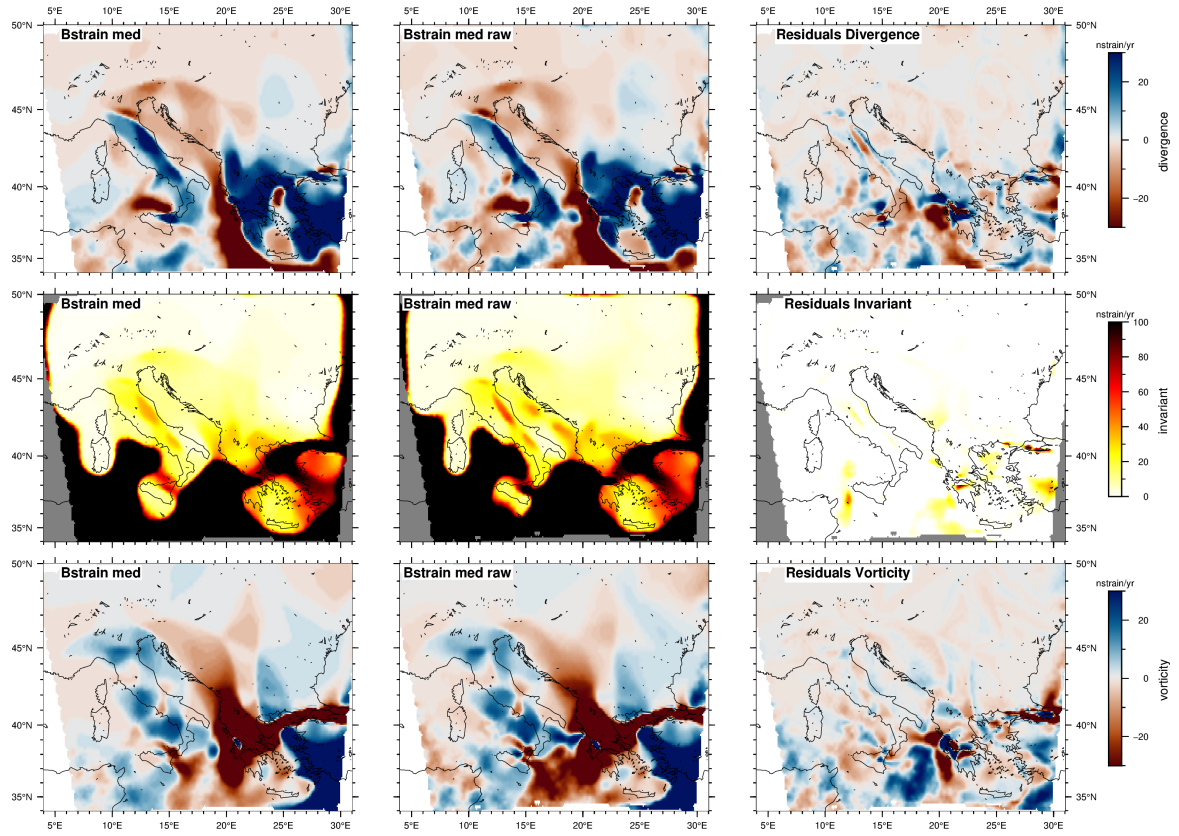

Fig. S9: Comparison of maps of median of divergence (top), invariant (middle) and vorticity (bottom) for our preferred calculation based on the cleaned velocity field proposed by (Piña-Valdés et al., 2022) (left) and BStrain outputs with the same parametrization but using the raw velocity field from (Piña-Valdés et al., 2022) that includes outliers (center). Right column shows residuals between both calculations.

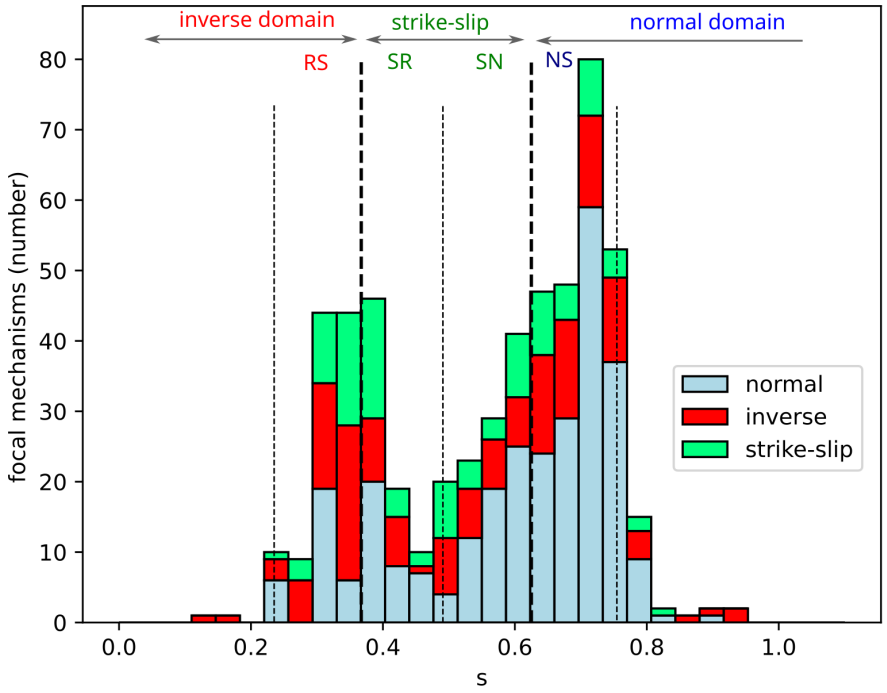

Fig. S10: Stacked histogram showing the number of focal mechanisms from the GCMT catalog shallower than 50 km (see figure 1) depending on their style (normal, reverse or strike-slip), as a function of the $s = \frac{3}{4} + \frac{1}{\pi} tan^{-1}(\epsilon_2/\epsilon_1)$ criteria. Vertical dashed lines stand for standards thresholds between reverse, normal and strike slip style. Thin dashed line separate domains where strike-slip coexist with normal (NS, SN) or reverse style (RS, SR) (Gordon and Houseman, 2015).